In situ observations and measurements during solidification of CuNi weld pools

Alexis Chiocca, Fabien Soulié, Frédéric Deschaux-Beaume, Cyril Bordreuil

In situ observations and measurements during solidification of CuNi weld pools

A. Chiocca*, F. Soulié, F. Deschaux-Beaume and C. Bordreuil

A two-scale *in situ* observation set-up has been used to investigate the physical phenomena around the solid/liquid interface in welding. A spot gas tungsten arc welding process is used to observe weld pool solidification phenomenon after arc extinction. The solidification front and the fluid flow in the weld pool have been observed at a microscale by a high speed camera. The whole weld pool and the surrounding base metal have been filmed at a macroscale by an infrared camera to estimate temperature fields around the weld pool and bead shape. A qualitative and quantitative dataset was extracted from these observations that involve useful results for further improvements of the understanding of weld solidification mechanisms and to enhance solidification models.

Keywords: Welding, Solidification, Fluid flow, Weld pool, Dendrite growth

Introduction

Critical regions for structural integrity of welded structures are often the fusion zones due to the difficulty to control microstructure in these areas. Microstructure is generated during solidification of the fusion zone. It is mainly controlled by thermal field evolution and fluid flow within the weld pool that depend on the heat source characteristics of the welding process. Kou[1] has shown for instance that a greater heat input on an aluminium alloy 6061 makes the microstructure transform from columnar grains to equiaxed grains in the centre part of the weld bead.

The microstructure generation is driven in the solidification temperature range at the trailing edge of the weld pool by grain growth in the liquid at the microscopic scale. The grain growth is influenced by solute segregation around the grains,[2] but also by factors depending on macroscopic field as G, the temperature gradient at the solid/liquid interface, and V_f, the solidification front velocity.[3,4] The morphology of the front is changed by decreasing the ratio G/V_f, from planar to cellular and finally dendritic.[5] The product $G.V_f$ influences the microstructure size: finer when it is high and coarser when it is low. The effect on the grain growth of the fluid flow in the weld pool near the solidification front has been studied theoretically and experimentally. Its influence on dendrite growth has been observed on columnar dendrites[6] or equiaxed dendritic grains.[2] An analytical model proposed by Gandin *et al.*[7] showed the dendritic growth rate increases with the fluid flow velocity, depending on the flow direction. However, these results were not yet confirmed by experimental data.

Conventional techniques used to explore dendritic growth involve the rapid quenching of a sample and its post-mortem micrograph examination. To investigate the effect of fluid flow on solidification mechanisms, alternative methods based on *in situ* measurements are necessary. Some studies have been recently engaged based on *in situ* observation using high speed camera,[8,9] infrared (IR) camera,[9,10] or X-ray diffraction[11,12] or transmission.[13] Hall *et al.*[14] visualised *in situ* dendritic growth at the border of a weld pool generated by a gas tungsten arc process to examine microstructure evolution. With the help of natural oxides present in the metal, Zhao[15] made PIV (particle image velocimetry) measurements to get the velocity field in the liquid.

The present work describes the experimental set-up designed to extract qualitative and quantitative data concerning physical phenomena within the weld pool and near the solid/liquid interface. The experimental set-up is developed to observe and measure data on spot gas tungsten arc welding (GTAW). The studied material is a Cu30Ni binary alloy with a controlled composition. This material is chosen for its simple solidification path (compared to stainless steels) that facilitates the analysis of solidification mechanisms. To access the fields controlling the microstructure, two scales of observation are used:

- A microscale to be able to observe the evolution of dendrites, the solidification front velocity and the fluid flow field close to the front.
- A macroscale in order to get the thermal field on the whole weld pool and in the solid part near the solid/liquid interface.

Experimental data obtained with this set-up are discussed with regard to the solidification mechanisms during welding.

Experimental

Experimental set-up

The tests consist in creating a spot weld with a GTAW machine for 6 s on a 1.6 mm thick and 70 mm diameter disc of Cu30Ni (Fig. 1). The energy range is chosen to

Laboratoire de Mécanique et Génie Civil, Université de Montpellier, CNRS, Montpellier, France

*Corresponding author, email alexis.chiocca@umontpellier.fr

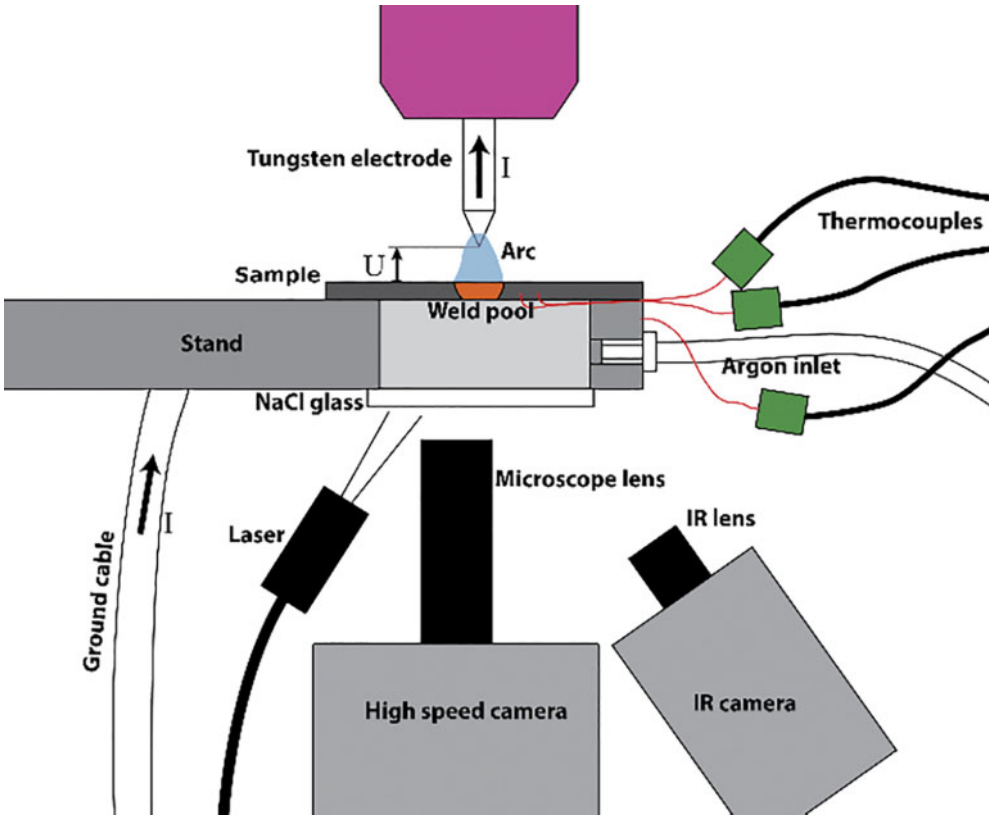

1 Experimental set-up and general disposition of measurement systems

produce a full penetrated weld pool. The argon gas shields the upper surface by the gas nozzle of the welding torch, and the back surface is protected by an inert box shielding against oxidation thanks to an argon circulation. A glass window under the box allows the visualisation of the backside of the weld; it provides a transmission of 90% on the whole range of wavelength (from 400 nm to 14 μm). The CuNi sample is maintained by a flange to avoid any distortions during the tests. The electrode employed, composed of tungsten with 2% of thorium, has a 2.4 mm diameter and a 30° grinding angle. Five energy inputs are chosen (Table 1) in order to appreciate the influence of energy level on temperature distribution, dendrite size and solidification rate.

The current I in the arc and the voltage U applied between the electrode and the sample are monitored. Field measurements are performed by two cameras, for microscale and macroscale observations (Fig. 1).

Microscale observation

Owing to the high solidification rate, the observation in the visible wavelengths is made by a near IR high speed camera placed under the sample. This position of the camera allows eliminating the problem of arc radiation. The camera is used with a microscope lens of magnification $\sim 7.1\times$, allowing the observation of the dendrites (Fig. 2). The observation area is chosen in order to visualise columnar dendrites. The scene is lit up by a 808 nm laser in order to obtain a good contrast both on the solid and on the liquid. Thus, the laser allows obtaining images of good resolution (512×512 pixels) with a high frame rate of 5000 fps.

Solidification rate

The solidification rate is measured by the moving velocity of the solidification front from video files. Raw images extracted from the video file are in a first step treated in contrast, brightness and gamma to reveal as much as possible the difference between the solid part and the liquid part. The solidification front, i.e. the contour between the solid and the liquid, can be drawn by differentiating solid and liquid textures (Fig. 2) with the help of dedicated contour detection algorithms.[16]

An example of treated image extracted from a film is illustrated on Fig. 2. The weld pool occupies the right hand side of the picture in black colour. On the left hand side, the solidified part and primary arms of dendrites growing into the liquid zone can be observed. In the lower part of the image, the small white spots are oxide particles travelling from between dendrites to the centre of the image. The big white spot in the bottom right hand corner is an oxide cluster floating and turning round on the weld pool.

The characteristics of the different images such as luminosity are nearly constant on a sample of 1000 images in a film taken at 5000 fps. For a larger sample, it is necessary to adapt the contrast, brightness and gamma adjustments. Before comparing the position of the solidification front on each image, it has been approximated by a least square method to an arc circle with a fixed centre

Table 1 Welding parameters for different tests

Test ID	1	2	3	4	5
Current/voltage	60 A/10 V	70 A/10 V	80 A/10 V	90 A/10 V	100 A/10 V

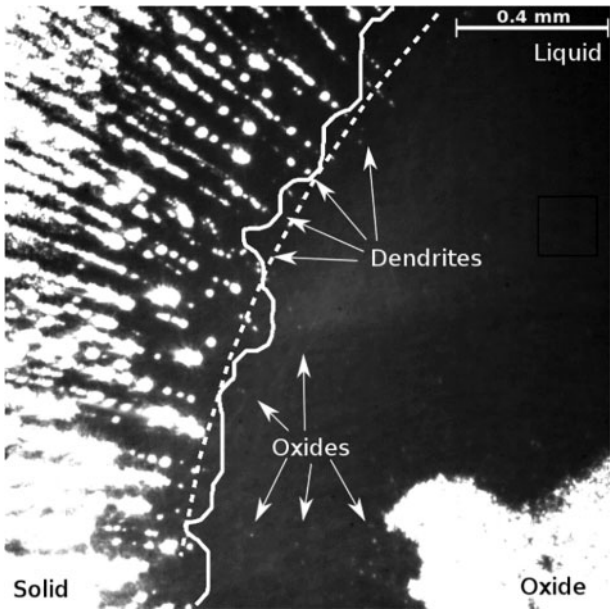

2 Raw contour determined from contour detection algorithm (white full line) and corresponding approximated arc circle (white dashed line)

(Fig. 2, in white dashed line). The front velocity is obtained with the slope of the curve describing the decreasing radius of the weld pool across time.

The measurements of solidification rates have to be done after the arc extinction, few milliseconds after the beginning of solidification when the solidification rate becomes stable, to reduce the variations for the comparison between tests.

Fluid flow velocity in weld pool

The samples of images extracted from video files to measure solidification rates are also treated to measure velocities of the fluid flow ahead of the solidification interface. As in the previous paragraph, contrast, brightness and gamma adjustments on the images are necessary to make visible floating particles appearing on the weld pool. These particles are mainly natural oxides. They follow the fluid flows in the weld pool and allow the measurement of the flowrates. Natural oxides already present in the base metal have been chosen as it is advised by Zhao[15] as being the best solution. Inoculation of foreign powders could also be a good solution to measure fluid flows but it could have an effect on the solidification mechanisms.

Two methods have been tested in order to achieve the flowrates: the PIV and the PTV (particle tracking velocimetry) processing. Considering the small number of particles observed on some video samples and the difficulty for the PIV algorithm to catch them, the PTV processing has been chosen. It gives more comparable data between the different video samples. When there are too few particles, the main disadvantage of the PIV processing consists in averaging velocities of the various particles, giving then results that are strongly dependent on the number of traceable particles in the window of interest.

The PTV processing results in a set of trajectories of particles flowing from the front to the centre of the weld pool (Fig. 3). Some particles are clearly flowing between

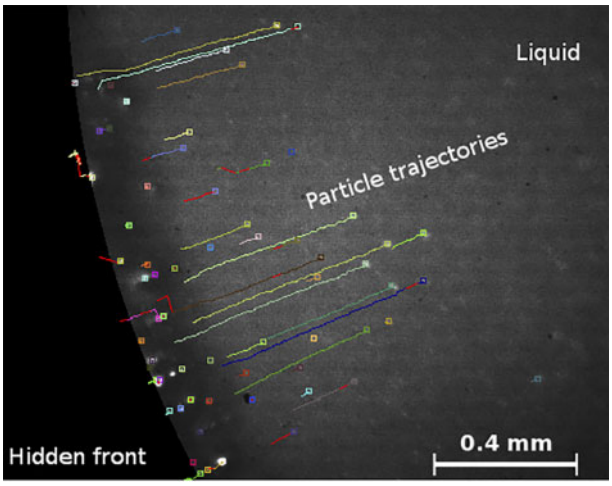

3 Trajectories of some particles calculated by PTV processing

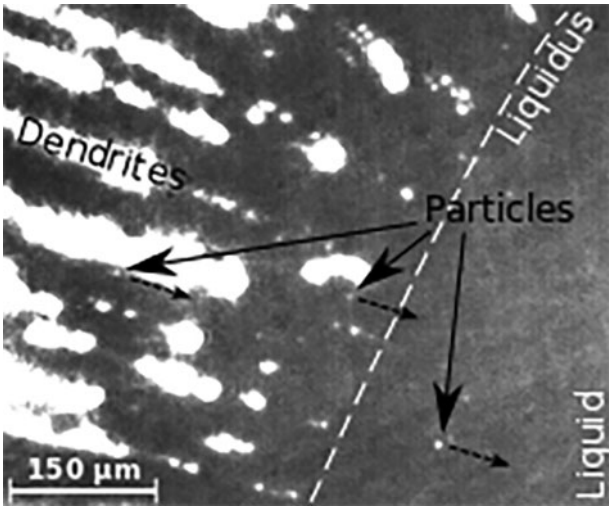

4 Particles coming from inside of semisolid zone between dendrites and flowing in direction of weld pool; their directions are plotted in dashed line arrows

the primary arms of dendrites before entering the weld pool (Fig. 4). PTV processing computes particle trajectories and allows the calculation of particles velocities, but these velocities might not be equivalent to the fluid flow velocity.

The size of the particles that follow the flow could be an issue and a factor of error. The bigger the floating particle is, the more it can slip on the surface instead of following the flow. Stokes number S_{tk} is a ratio of crucial importance for evaluating the accuracy of the PTV method: $S_{tk} = \rho d^2 u_p / \mu L$ with $d = 10\,\mu m$ (the size of a particle), $u_p = 100$ mm s^{-1} (the velocity of the particle), $L = 2.33$ mm (the characteristic length of the fluid flow corresponding in this case to the minimum radius of the weld spot), $\mu = 3.1 \times 10^{-3}$ Pa.s (the viscosity of the liquid material[17]) and $\rho = 8.94 \times 10^3$ kg m^{-3} (the density of Cu30Ni).[18] It quantifies the ability of tracer particles to adapt their velocity to the instantaneous velocity of surrounding flow. It is generally admitted that for $S_{tk} \ll 1$, the slipping is not significant.[19] In our tests, the calculated value is $\sim 12.7 \times 10^{-3}$, so the tracer accuracy is acceptable and particles are supposed to follow fluid streamlines closely.

After getting out from the front, particles gather in the middle of the weld pool and are seen turning round as a united block. The rotation of the particles in the middle of the weld pool could be the effect of a vortex when the flow goes up in the centre (Fig. 8).

Macroscale observations and calibration

At the macroscale, the thermal field is needed to reach the temperature gradient near the solidification front.

The determination of the thermal field is done by two coupled devices: thermocouples and an IR camera (Fig. 1). Two thermocouples are placed along a radius of the sample at 10 and 15 mm from the centre. Another one is placed in the flange to control its temperature and prevent overheating that could preheat the plate and affect the results. The IR wavelength range of measurement is located between 8 and 14 μm, corresponding to long wavelength IR range.

The determination of the thermal fields from IR camera requires a calibration with the help of the two first thermocouples placed near the centre of the sample. The grey level provided by each pixel of the camera gives a value proportional to the real luminance of the observed object. The Planck law is used to link temperature to luminance on all images of the video on the whole sample. The sample is assumed to be a grey body with a constant emissivity for the Plank law calculation. The final relation for each pixel is $E_{GL} = \varepsilon/k\,\mathrm{Pl}(T) + C$, where E_{GL} is the grey level of each pixel, ε is the emissivity of the grey body, k is the proportionality factor between the grey level and the luminance, C is a constant from the relation between E_{GL} and the luminance, and Pl(T) is the Planck law. The calibration is achieved by correlating the temperatures measured by the two thermocouples with the grey levels of pixels of the IR image corresponding to thermocouple locations. The parameters to be found by this correlation are ε/k and C. The thermal field and the resulting temperature along a radius of the plate are presented on Fig. 5.

Because of the difficulty to precisely locate the weld pool border, which appears blur in the raw image, the temperatures estimated at the weld pool border are always below the liquidus temperature of 1520 K and differ between the various tests (Fig. 5). However, the temperature gradients change slowly around the weld pool border and are less sensible to the localisation accuracy, as it can be seen in Fig. 5.

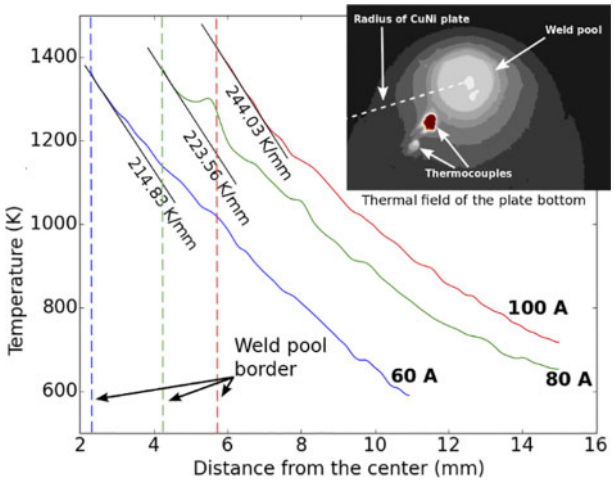

5 Temperature variations along radius of CuNi sample from border of weld pool to border of sample; these temperatures are measured at arc extinction corresponding to beginning of solidification

Results and discussion

The main results deduced from the various tests are summarised in Table 2. Note that only the value of current changes between each test. All the other parameters are assumed constant.

Thermal results

As expected, the energy input influences the weld pool size but also the weld pool shape. At low energy, the weld pool top radius is greater than the weld pool bottom radius, but at higher energy, the difference becomes smaller. The temperature in the weld pool is more homogeneous in the case of high energy. It is probably due to a higher global convection as underlined by the higher maximal velocities of the particles with higher energies (Table 2). It can also explain the weld pool shapes.

The thermal gradient, around the solidification front at the arc extinction, seems to increase slightly when the welding current increases, but remains around the value of 250 K mm^{-1} (Table 2 and Fig. 5). It shows that the heat flow through the border of the weld pool is not very different between the various tests. It is confirmed by the rather constant cooling rate ($G.V_f$) measured for all tests (Table 2). Note that the thermal gradient at the solidification front is extracted only at the beginning of the solidification. It has been unfortunately impossible to follow its evolution when the weld pool radius decreases because of the lack of accuracy of the IR camera for small weld pools.

Fluid flow and solidification

Solidification front

The solidification front velocity tends to decrease with the increase of heat input (Fig. 7). The exchange surface between the weld pool and the unmelted material increases when the heat input increases; the weld pool diameter for the highest energy is about twice the lowest energy one (Table 2). This increase of exchange surface, coupled with the rather constant temperature gradient measured at the solid/liquid interface for all the tests, enhances the global heat flow through the weld pool border for high energy that should favour the cooling of the weld pool. However, the higher energy contained in the weld pool, which has a volume more than four times higher for the maximal energy than for the minimal one at the arc extinction, can explain the lower solidification velocities measured for the high heat inputs.

Figure 6 shows the relation of the solidification front velocity with the thermal gradient at the solidification front, measured after the arc extinction for the various tests. The grey level of the points is proportional to the energy input. The increase in energy input tends to increase the ratio G/V_f and has not any significant effect on the cooling rate $G.V_f$. According to the diagram proposed by Kurz and Fisher,[5] the increase in energy then should lead more easily to a cellular growth, whereas a lower energy should lead to a columnar or equiaxed dendritic growth. However, in the main part of our observation area (Fig. 2), the solidification mode is

Table 2 Resulting weld pool (WP) sizes, temperature gradients at weld pool border at beginning of solidification, maximal particle velocities, front velocities and cooling rates for different tests

Test ID	Top WP diameter (D_t)	Bottom WP diameter (D_b)	Temperature gradient	Max. particle velocity	Front velocity	Cooling rate
1	6.35 mm	4.65 mm	242 K mm^{-1}	36 mm s^{-1}	3.7 mm s^{-1}	906 K s^{-1}
2	7.97 mm	6.70 mm	255 K mm^{-1}	61 mm s^{-1}	3.5 mm s^{-1}	903 K s^{-1}
3	9.75 mm	9.75 mm	224 K mm^{-1}	50 mm s^{-1}	2.8 mm s^{-1}	630 K s^{-1}
4	11.05 mm	10.26 mm	302 K mm^{-1}	73 mm s^{-1}	2.7 mm s^{-1}	808 K s^{-1}
5	12.02 mm	11.36 mm	244 K mm^{-1}	80 mm s^{-1}	2.8 mm s^{-1}	693 K s^{-1}

always a columnar dendritic growth, whatever the heat input. This is probably because the variations of the temperature gradient and the solidification front velocity for the various tests are not great enough to see any morphological transition. In Fig. 6, the points characterising all experiments are located in the columnar dendritic solidification mode area in the Kurz and Fisher diagram,[5] so it is coherent with the observed columnar dendrites.

However, observations made at the back side at the end of solidification show, in the centre of the weld pool, grains growing into the liquid, whereas the solidification front has not reached the centre. It might be equiaxed grains nucleating in the liquid ahead of the solidification front because of a decreasing ratio G/V_f at the end of solidification. Unfortunately, this assumption could not be confirmed by experimental measurements because the IR camera is not accurate enough for extracting G and V_f when the weld pool diameter is low.

According to Kurz and Fisher,[5] the dendritic spacing mainly depends on the cooling rate in the solidification temperature range. Measurements on the primary dendrite arms spacing show only little variations $\sim$75 μm for the various tests, which is in agreement with the similar cooling rates observed in these experiments.

Fluid flow in spot welding

The observation of particle trajectories seems to indicate a laminar flow: all the particles move in the same direction and slow down at the same speed. The Reynolds numbers, computed with weld pools radius as characteristic length, are in agreement with this observation. The values are from $\sim$150 to 1250, and sometimes can rise up to 1500 in the vicinity of the solidification front. Fluid flow velocities in the weld pool have been measured at three different distances from the solidification front (Fig. 7). Two tendencies can be observed from these measurements. First, the velocity of the fluid flow increases with the increase of the energy input, whatever the distance to the front. Second, the velocity decreases while reaching the centre of the weld pool.

The fluid flow observed in the back side of the sample is partially controlled by Marangoni convection due to the variations of the surface tension with temperature that has already been observed on analogous metal materials.[20]

The Marangoni number is defined as $M_g = -\frac{d\sigma}{dT}\frac{1}{\eta\alpha}L_C\Delta T$, where σ is the surface tension, T is the temperature, η is the viscosity, α is the thermal diffusivity, L_C is the characteristic length and ΔT is the temperature range on the characteristic length. Owing to the increasing energy, the characteristic length L_C increases, leading to higher Marangoni convection.

Note that the observations made by the high speed camera give only two-dimensional (2D) information of a three-dimensional (3D) phenomenon. One can explain the 3D flow in the following way: the particles observed on the back surface between the columnar dendrites come from the top side or the deep of the weld pool, flow between dendrites to converge to the centre of the weld pool, and return in the deep or in the top (Fig. 8). Because Marangoni effect acts also on the top side of the weld pool, depending on the thermal fields on this side,

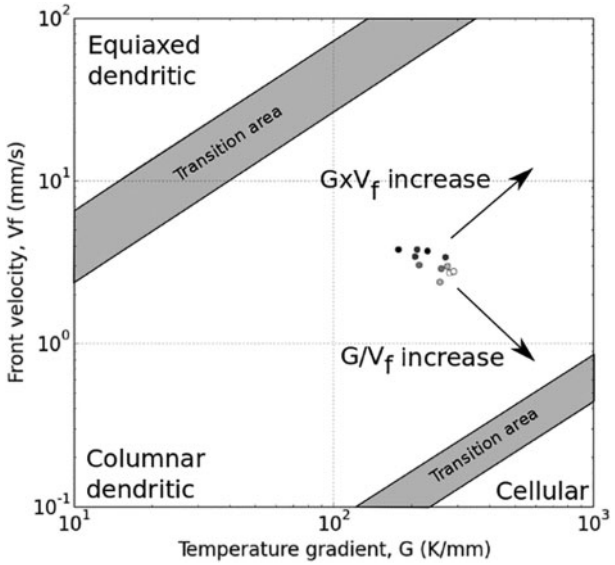

6 Position of different tests in growth velocity versus temperature gradient diagram; light spot means higher energy input and dark spot means lower energy input

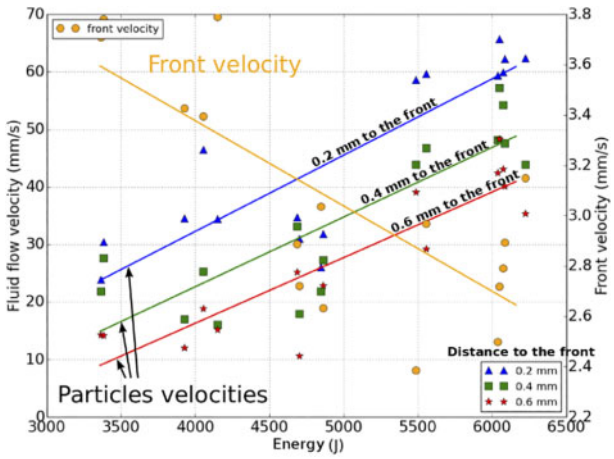

7 Variations of solidification front velocity and particle velocity at different distances to front, with respect to energy input

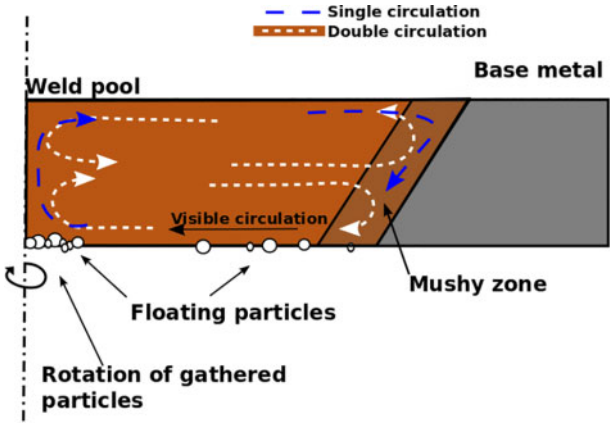

8 Fluid flow observed by camera (full arrows) and supposed 3D fluid flows according to observations (dashed arrows)

the flow could have a single or a double circulation, as it has been predicted by Fan *et al.*[21]

According to these experimental results, the increase of energy input leads to an increase of fluid flow velocity in the weld pool and a decrease of the solidification front velocity. To take into account the effect of the fluid flow on the solidification velocity, Gandin *et al.*[7] developed a model based on a 'boundary layer' around the dendrite tip in which the solute flow is diffusion controlled, whereas the composition is supposed homogeneous outside of this layer due to the fluid flow. According to this model, the thickness of the boundary layer decreases with the fluid flow when its direction is opposite to the growth direction, leading to an increase in solidification velocity. However, they supposed that the boundary layer has an infinite thickness when the fluid flow is in the same direction than the dendrite growth, as in the case of our experiments on the backside of the weld pool. The solidification regime is then, according to this model, purely diffusion controlled, without influence of the fluid velocity. In a purely diffusive regime, the increase in the ratio G/V_f implies a decrease in constitutional undercooling, which leads to a decrease in solidification velocity.[1,22] The increase of this ratio when the heat input increases observed in our experiment (Fig. 6) then partly explains the solidification velocity evolution, regardless of the flow velocity. However, the values of the solute Péclet number $Pe_S = \frac{r.(V_f+u)}{D}$, which compare diffusive and convective mass transfers, between 5 and 100, where r is the radius of the dendrite tip, D is the diffusion coefficient of Cu in the material at the liquidus temperature, and u is the fluid flow velocity at the dendrites tip, indicating that the convection dominates the diffusion. The fluid flow then should have a role on the solute flow and probably also on the solidification velocity, even when its direction is the same than the growth direction. Note also that due to the 3D flow, the fluid flow in the core or in the top side of the weld pool is opposite to the growth direction (Fig. 8). This should increase the solidification velocity according to Gandin's model, so it is possible the solidification velocity varies in the thickness of the sample. Concerning the thermal flow, the thermal Péclet number is very low at the microscale ($Pe_{th} = \frac{r.(V_f+u)}{\alpha} << 1$, where α is the thermal diffusivity), indicating that the conduction drives the thermal flow, which is very fast compared to solute flow, and then should not have a great influence on the growth kinetic.

However, at the macroscale, the thermal Péclet number is ~ 50 ($Pe_{th} = \frac{R_b.V_f}{\alpha}$), where R_b is the weld pool radius, so the thermal convection strongly contributes to change the size and the shape of the weld pool, which should explain the shape variations of the weld pool when the heat input increases (Table 2).

Conclusions

A dedicated experimental set-up allowing *in situ* measurements with observation at a macroscale and at a microscale during solidification in welding has been designed. It makes possible to observe and quantify key parameters of solidification phenomena such as solidification rate, dendrite growth velocity, and flow direction and velocity in the weld pool and in the semisolid zone.

The different measurements show that a higher energy input leads to higher fluid flow velocity, but lower dendrite growth velocity, even if the temperature gradient stay unchanged at the solid/liquid interface. However, the fluid motion stays complex and a lack of information still remains in the inside of the weld pool.

The results presented here provide a useful database to improve the understanding of the weld pool solidification mechanisms and to validate or improve numerical models. A study on a moving weld pool could provide results closer to real welding conditions.

References

1 S. Kou: 'Welding metallurgy'; 2003, Hoboken, NJ, John Wiley & Sons Inc. 4
2 J. A. Dantzig and M. Rappaz: 'Solidification'; 2009, Switzerland, EPFL Press.
3 M. Tong, G. Duggan and D. J. Browne: 'Modelling the creation and destruction of columnar and equiaxed zones during solidification and melting in multi-pass welding of steel', *Comput. Mater. Sci.*, 2015, **97**, 285–294.
4 A. Kidess, M. Tong, G. Duggan, D. J. Browne, S. Kenjereš, I. Richardson and C. R. Kleijn: 'An integrated model for the post-solidification shape and grain morphology of fusion welds', *Int. J. Heat Mass Transfer*, 2015, **85**, 667–678.
5 W. Kurz and K. Fisher: 'Fundamentals of solidification', 305; 1992, Switzerland, Trans Tech Publications Ltd. 6
6 S. Boden, S. Eckert and G. Gerbeth: 'Visualization of freckle formation induced by forced melt convection in solidifying GaIn alloys', *Mater. Lett.*, 2010, **64**, (12), 1340–1343.
7 C. A. Gandin, G. Guillemot, B. Appolaire and N. T. Niane: 'Boundary layer correlation for dendrite tip growth with fluid flow', *Mater. Sci. Eng. A*, 2003, **A342**, (1–2), 44–50.
8 K. Li, Z. Wu and C. Liu: 'Measurement and calculation of plasma drag force in arc welding based on high-speed photography technology and particle dynamics', *Mater. Des.*, 2015, **85**, 97–101. 5
9 P. von Witzendorff, S. Kaierle, O. Suttmann and L. Overmeyer: 'Using pulse shaping to control temporal strain development and solidification cracking in pulsed laser welding of 6082 aluminum alloys', *J. Mater. Process. Technol.*, 2015, **225**, 162–169.
10 J. Chen, X. Yu, R. G. Miller and Z. Feng: 'In situ strain and temperature measurement and modelling during arc welding', *Sci. Technol. Weld. Join.*, 2015, **20**, (3), 181–188.
11 W. U. Mirihanage, M. Di Michiel, A. Reiten, L. Arnberg, H. B. Dong and R. H. Mathiesen: 'Time-resolved X-ray diffraction studies of solidification microstructure evolution in welding', *Acta Mater.*, 2014, **68**, 168–259.
12 W. U. Mirihanage, M. Di Michiel and R. H. Mathiesen: 'Ultrafast in-situ X-ray studies of evolving columnar dendrites in solidifying steel weld pools', *Mater. Sci. Eng.*, 2015, **84**, (1), Article ID. 012029.
13 S. Li, G. Chen, S. Katayama and Y. Zhang: 'Relationship between spatter formation and dynamic molten pool during high-power deep-penetration laser welding', *Appl. Surf. Sci.*, 2014, **303**, 481–488.

14 A. C. Hall, G. A. Knorovsky, C. V. Robino, J. Brooks, D. O. Maccallum, M. Reece and G. Poulter: 'Characterizing the microstructure of a GTA weld in-process using high-speed, high magnification, digital imaging', Eleventh International Conference on Computer Technology in Welding, Gaithersburg, MD U.S. Dept. of Commerce, Technology Administration, National Institute of Standards and Technology (NIST); 2002. 7
15 C. X. Zhao and A. S. M. Proc: 'Experimental characterization of GTA weld pool surface flow using PIV', *Int. Conf: Trends Weld. Res.*, 2009, 201–210.
16 E. Romero, J. Chapuis, C. Bordreuil, F. Soulie and G. Fras: 'Image processing and geometrical analysis for profile detection during pulsed gas metal arc welding', *P.I. Mech. Eng. B.J. Eng. Manuf.*, 2013, **227**, (3), 396–406.
17 N. Chakraborty: 'The effects of turbulence on molten pool transport during melting and solidification processes in continuous conduction mode laser welding of copper–nickel dissimilar couple', *Appl. Therm. Eng.*, 2009, **29**, (17218), 3618–3631.
18 J. Brillo and I. Egry: 'Density determination of liquid copper, nickel, and their alloys', *Int. J. Thermophys.*, 2003, **24**, 1155–1170.
19 C. Tropea, A. L. Yarin and J. F. Foss: 'Springer handbook of experimental fluid mechanics'; 2007, Berlin, Springer-Verlag.
20 S. Kou: 'Fluid flow and solidification in welding: three decades of fundamentals research at the university of Wisconsin', *Weld. J.*, 2012, **91**, 287s–302s.
21 H. G. Fan, H. L. Tsai and S. J. Na: 'Heat transfer and fluid flow in a partially or fully penetrated weld pool in gas tungsten arc welding', *Int. J. Heat Mass Transfer*, 2000, **44**, 417–428.
22 O. Hunziker, D. Dye and R. C. Reed: 'On the formation of a centreline grain boundary during fusion welding', *Acta Mater.*, 2000, **48**, (17), 4191–4201.